

NATIONAL AERONAUTICS AND SPACE ADMINISTRATION

N73-30838

*Technical Memorandum 33-632*

*Slosh Testing of a Spherical Mercury Propellant  
Tank With Positive-Expulsion Diaphragm*

*R. G. Ross, Jr.*

*J. R. Womack*

**CASE FILE  
COPY**

**JET PROPULSION LABORATORY  
CALIFORNIA INSTITUTE OF TECHNOLOGY  
PASADENA, CALIFORNIA**

July 15, 1973



NATIONAL AERONAUTICS AND SPACE ADMINISTRATION

*Technical Memorandum 33-632*

*Slosh Testing of a Spherical Mercury Propellant  
Tank With Positive-Expulsion Diaphragm*

*R. G. Ross, Jr.*

*J. R. Womack*

**JET PROPULSION LABORATORY  
CALIFORNIA INSTITUTE OF TECHNOLOGY  
PASADENA, CALIFORNIA**

July 15, 1973

Prepared Under Contract No. NAS 7-100  
National Aeronautics and Space Administration

PREFACE

The work described in this report was performed by the Applied Mechanics Division of the Jet Propulsion Laboratory.



## CONTENTS

I.	Introduction . . . . .	1
II.	Test Objective and Scope . . . . .	1
III.	Approach . . . . .	2
IV.	Apparatus and Instrumentation . . . . .	3
	A. Propellant Tank . . . . .	3
	B. Sloshing Apparatus and Instrumentation . . . . .	4
V.	Test Results and Discussion . . . . .	4
	A. Preliminary Test with Water . . . . .	4
	B. Mercury Slosh Test (17.5% Ullage) . . . . .	6
VI.	Dynamic Property Determination . . . . .	8
	A. Parameter Estimation From Nyquist Plots . . . . .	8
	B. Parameter Optimization by Least Squares . . . . .	9
	C. Parameter Estimates for Tested Tank . . . . .	11
VII.	Summary and Recommendations . . . . .	13
	Appendix: Derivation of Theoretical Co-Quad Response . . . . .	15
	References . . . . .	20

## FIGURES

1.	SEPST Program propellant tank design . . . . .	21
2.	Test tank mounted in sloshing apparatus . . . . .	22
3.	Shaker control and data processing console . . . . .	23
4.	Test tank with water (17.5% ullage) . . . . .	24
5.	Static diaphragm shapes with mercury for various ullages . . . . .	25
6.	Quadrature response of test tank with mercury . . . . .	29
7.	Approximate mode shapes for mercury resonances . . . . .	29
8.	Nyquist plot for 0.05 g excitation level . . . . .	30
9.	Nyquist plot for 0.1 g excitation level . . . . .	30

CONTENTS (contd)

FIGURES (contd)

10.	Nyquist plot for 0.3 g excitation level . . . . .	31
11.	Nyquist plot for 0.5 g excitation level . . . . .	31
12.	Typical Nyquist plot for single-degree-of-freedom system . . . . .	32
13.	Typical Nyquist plot for multiple-degree-of-freedom system . . . . .	32
14.	Initial linear system fit for 0.05 g data . . . . .	33
15.	Initial linear system fit for 0.1 g data . . . . .	33
16.	Optimized linear system fit for 0.1 g data . . . . .	34
17.	Initial single-degree-of-freedom fit for 0.3 g primary resonance . . . . .	34
18.	Optimized linear system fit for 0.3 g data . . . . .	35
19.	Optimized linear system fit for 0.5 g data . . . . .	35
20.	Natural frequency versus excitation level . . . . .	36
21.	Damping ratio vs excitation level . . . . .	37
22.	Mass fraction vs excitation level . . . . .	38
A1.	Dynamic model of tank/fluid system . . . . .	39

## ABSTRACT

A preliminary investigation was conducted to evaluate the lateral slosh characteristics of a 23-cm- (9-in. -) diam mercury propellant tank with a positive-expulsion diaphragm and 17.5% ullage. Data are presented for tank sinusoidal acceleration levels between 0.05 and 0.5 g at frequencies ranging from 5 to 50 Hz. Results indicate that the slosh characteristics are highly nonlinear at acceleration levels approaching those in flight, and depend heavily on the shape and stiffness of the diaphragm. Nyquist plots of driving force over acceleration are shown to be a useful tool for determining natural frequency, damping, and modal mass characteristics. A computerized nonlinear least-squares method for extracting the modal parameters from the Nyquist plots is described and results of applying the method are presented.



## I. INTRODUCTION

The Solar Electric Propulsion (SEP) Thrust Subsystem Engineering Model Technology Program is aimed at the design, development, and functional test of an engineering model of a solar electric propulsion subsystem for a SEP spacecraft. A portion of the Program is centered on the tank that contains the mercury propellant for the ion engines. Current emphasis is on a spherical tank equipped with an elastomeric diaphragm for the positive expulsion of the mercury.

An important part of the development of the tank design is the evaluation of the slosh characteristics of a partially off-loaded tank. This report describes the results of a study of the lateral slosh characteristics of a 23-cm- (9-in. -) diam prototype mercury propellant tank developed during the Solar Electric Propulsion System Technology (SEPST) Program (Ref. 1). The general configuration of the tank is indicated in Fig. 1.

## II. TEST OBJECTIVE AND SCOPE

The primary objective of the test program was to gain a preliminary understanding of the dynamic slosh characteristics of the prototype tank. Of particular interest was the dynamic behavior of the fluid at vibration levels approaching those anticipated during the launch of an SEP spacecraft aboard a Titan-III or shuttle launch vehicle. A secondary objective, established during the course of the study, was the development of an improved method for reducing the experimental slosh dynamics data and constructing equivalent mechanical models of the sloshing fluid.

Early in the study a number of items were identified as important slosh parameters. These are listed below:

- (1) Gravity field (1 g vs quasi-static launch).
- (2) Tank diameter.
- (3) Ullage volume.
- (4) Ullage fluid (gas vs liquid).
- (5) Ullage pressure level.
- (6) Diaphragm stiffness (thickness and material).
- (7) Dynamic excitation level.
- (8) Dynamic excitation direction (vertical vs lateral).

Because of programmatic constraints it was necessary to limit the study to a single tank configuration and ullage volume. Emphasis was placed on establishing the general slosh behavior as a function of excitation level, and, in particular, evaluating the natural frequencies, damping, and modal masses of the lateral slosh modes at sinusoidal excitation levels between 0.05 and 0.5 g peak. It was assumed that follow-on work would be performed to evaluate the slosh problem further. Determining the scope of future test requirements and the generation of general computerized data reduction techniques compatible with future testing requirements was considered an important part of the current study.

The test configuration is summarized below:

- (1) Tank: 23-cm-diam sphere.
- (2) Diaphragm: 1.6-mm-thick neoprene.
- (3) Fluid: mercury.
- (4) Ullage volume: 17.5%.
- (5) Ullage fluid: air.
- (6) Ullage pressure:  $10^5$  N/m<sup>2</sup> (1 atm).

### III. APPROACH

The problem of determining the dynamic properties of a sloshing fluid is basically one of system identification from measured response data. The

usual approaches are based on the measured amplitude response of the fluid to steady-state sinusoidal base excitation.

Using a technique described in Ref. 2, the sloshing fluid was represented as a rigid mass plus a number of uncoupled single-degree-of-freedom oscillators, each representing a lateral slosh mode. Each oscillator is described in terms of its natural frequency, damping ratio, and mass. The problem of determining the dynamic properties of the sloshing fluid was thus reduced to determining the natural frequency, damping, and mass associated with each dominant slosh mode. The rigid "residual" mass of the fluid equals the total fluid mass minus the sum of the slosh masses.

Though methods for determining the dynamic properties (natural frequency, damping, and mass) of multiple-degree-of-freedom systems are generally based on system amplitude response to steady-state sinusoidal excitation, it is desirable also to make use of the phase relationship between the driving force and the system response. When both amplitude and phase data are available, it is possible to generate Co-Quad or Nyquist plots that greatly aid the determination of the dynamic properties.

In the current program the propellant tank was excited with a constant amplitude sinusoidal base acceleration at frequencies ranging from 2 to 50 Hz. The driving force at the base, the base acceleration, and the phase between them were recorded. These data were plotted in the form of Nyquist phase-plane plots. The dynamic properties were then extracted from the Nyquist plots using computerized curve fitting techniques. The data reduction technique is described in greater detail in Section VI.

#### IV. APPARATUS AND INSTRUMENTATION

##### A. Propellant Tank

The tank used in the slosh test was a modified version of the 23-cm-diam SEPST prototype tank described in Ref. 1. To allow the slosh motion to be observed, the tank was fitted with a clear Lucite upper hemisphere and a grid pattern was painted on the neoprene diaphragm.

## B. Sloshing Apparatus and Instrumentation

To provide for near-frictionless lateral motion, the tank was supported on a carriage free to roll on linear ball bushings. The tank/carriage assembly was driven by an Unholtz-Dickie Model 4 electrodynamic shaker with a 10-cm (4-in.) stroke and 670-N (150-lb) force capability. An accelerometer was positioned on the carriage for acceleration measurement, and a precision load cell was positioned between the shaker and the carriage for force measurement. The initial configuration with two shakers is shown in Fig. 2. Only one shaker was used during most of the testing.

Signals from the accelerometer and load cell were fed into the shaker control and signal processing console shown in Fig. 3. Both signals were conditioned through a tracking filter to strip off response harmonics not at the driving frequency. The amplitude and phase data were then printed on the teletype along with the driving frequency.

All moving components of the shaking apparatus were carefully weighed. Calibration on the entire system was then verified by initially shaking the tank in a completely filled condition, and noting that the force over acceleration agreed with the measured system weight, and that the phase angle was zero.

## V. TEST RESULTS AND DISCUSSION

### A. Preliminary Test With Water

Preceding the system verification test with the tank completely filled with mercury, a test was conducted using water in place of mercury. This test was primarily aimed at debugging the test procedures and equipment before introducing the certain degree of hazard associated with the mercury. However, the test using water also provided some significant observations.

An 82.5% filled (17.5% ullage) condition was used in the water slosh test. This is the same level used later in the mercury tests. As shown in Fig. 4, the diaphragm was generally spherical in shape and did not have the concave dimple exhibited when the water was replaced with the same volume of mercury. The shape of the diaphragm when 82.5% filled with mercury is essentially that shown in Fig. 5 for the 20% ullage condition.

In both cases, water and mercury, it is clear that the diaphragm significantly alters the free surface of the fluid by supporting the fluid away from the tank wall. As a result the classical first free surface slosh mode, which is typified by a general fluid pendulum motion, does not occur. At low vibration levels (less than 0.1 g) the system stiffness appears to be almost entirely controlled by the stiffness and shape of the diaphragm. The first mode shapes for the water and mercury were entirely different. The first slosh mode for the water was a first cantilever mode motion of the entire free surface hemisphere at approximately 27 Hz, over ten times the theoretical resonant frequency for the same fluid volume with a free surface.

The first slosh mode with the mercury was a wave action mode associated with a rolling of the diaphragm dimple from side to side at about 2.5 Hz. However, the dominant mode was the second mode, which corresponded to flexing of the side walls of the diaphragm at about 9 Hz. The mercury slosh results are described in greater detail later.

From a comparison of the slosh behavior of the two fluids with the theoretical free surface behavior, several conclusions can be drawn.

- (1) Theoretical models available for free surface sloshing do not appear to provide a reasonable means of predicting slosh modes and frequencies with the tested diaphragm.
- (2) Because the slosh modes and frequencies are apparently highly dependent on the diaphragm stiffness and deformed shape, the slosh frequencies should not depend on the vertical gravity field in the classical  $\sqrt{g}$  manner. However, the difference between the water and mercury mode shapes and frequencies suggests that the slosh behavior could be a strong function of the acceleration field strength.
- (3) Because of the inappropriateness of the free surface slosh theory, direct means for extrapolating to the behavior of different ullages, larger tanks, different diaphragms, and different acceleration fields are not currently available. As a result emphasis will have to be placed on acquiring empirical slosh data.

## B. Mercury Slosh Test (17.5% Ullage)

Following the system verification tests, the tank was filled with 67 kg (147 lb) of mercury to give an 82.5% filled condition. Tests were run using constant acceleration sinusoidal base excitations of 0.05, 0.1, 0.3 and 0.5 g peak, at frequencies ranging from 2 to 50 Hz. Though the slosh was only moderately sensitive to acceleration level at both acceleration extremes, there was an abrupt change in the system behavior between 0.1 and 0.3 g. This change is indicated in the quadrature response plots presented in Fig. 6.

The quadrature response plots are plots of the normalized component of the driving force, which is 90 deg out of phase with the driving acceleration. Since the force associated with driving the rigid tank and nonresonant fluid mass is zero or 180 deg out of phase with the driving acceleration, it does not influence the quadrature response. For this reason the peaks in the quadrature response more accurately represent the natural slosh frequencies, than do peaks in the total response. In Fig. 6 the quadrature force is normalized by dividing by the total fluid mass times the acceleration level. The normalized quadrature force can thus be considered as a force amplification factor relative to the reaction force required if the fluid were a rigid mass.

The mode shapes observed to correspond to the resonant peaks in Fig. 6 have been sketched in Fig. 7. Because of the inherent uncertainties in visually observing mode shapes, the sketches are intended to provide only a qualitative insight into the slosh phenomena. As indicated, the first slosh mode at the lower vibration levels differed significantly from the first mode at the higher levels. At the 0.05- and 0.1-g levels the first mode consisted of a surface wave associated with a rolling of the diaphragm dimple from side to side. This mode was highly unstable and quickly coupled with liquid swirl. At acceleration levels above 0.2 g the diaphragm was unable to maintain its dimpled shape as the frequency was raised above 3 Hz. At this frequency the tank entered a completely new first mode resonance associated with a deformed diaphragm shape. In this mode a large fraction of the contained mercury "flopped" from side to side, stretching the diaphragm and impacting the wall of the tank. The mode did not exhibit liquid swirl, but became unstable above 5 Hz and disappeared with a jump back to the original dimpled diaphragm equilibrium shape.

Above 5 Hz the slosh response was similar at all excitation levels with a general trend toward higher damping and lower natural frequencies with increasing excitation level. As indicated in Fig. 7 the higher modes can be considered as a series of modes associated with vibration of the vertical side wall of the diaphragm. The first side wall mode (second tank mode) is the dominant mode at low excitation levels.

A number of conclusions can be drawn from these observations.

- (1) The dynamic behavior of the sloshing tank is highly nonlinear at acceleration levels approaching those in flight.
- (2) The slosh modes of the tested tank appear to be highly associated with the shape of the diaphragm. This implies that the modes should be a strong function of any parameter that reflects a change in diaphragm shape. Examples are ullage volume and the vertical acceleration field, which effects the hydrostatic fluid pressure on the sides of the protruding diaphragm at low ullages.
- (3) Because the primary mode at high acceleration levels is associated with a different, deformed diaphragm shape, one can conclude that the measured higher order modes (which correspond to the static undeformed shape) can not occur simultaneously with the primary mode. In fact, there probably exists a different set of higher order modes associated with the deformed diaphragm shape.
- (4) Because the high-level response was significantly different from the low-level response, future testing needs to be conducted at flight levels to insure that data are applicable to flight analyses.
- (5) During the test program the prototype tank was subjected to a number of hours of excitation at the 0.5-g level. This level slightly exceeds anticipated qualification test levels in the critical frequency range below 10 Hz. Because the tank and diaphragm exhibited no failures during the test program, an important additional conclusion is that the prototype diaphragm is structurally quite satisfactory.

## VI. DYNAMIC PROPERTY DETERMINATION

### A. Parameter Estimation From Nyquist Plots

Though the quadrature response plots presented in Section V graphically display the resonant frequencies, there are other data formats that more readily allow the extraction of slosh mass and damping information. The Nyquist phase plane plot has been found to provide an ideal format for complete dynamic property determination and was adopted in this study. Nyquist plots of the slosh response at each of the excitation levels are provided in Figs. 8 through 11. The ordinate of these plots is the same normalized quadrature (Quad) response that was plotted in Fig. 6. The abscissa is the normalized coincident (Co) response, in other words, the component of the fluid reaction force that is in phase with the driving acceleration. Precisely, it is the in-phase component of the fluid reaction force (total in-phase force minus rigid fixture and tank accelerating force) divided by the total fluid mass times the acceleration level. The Nyquist plots thus can be interpreted as phase plane plots of the reaction force amplification factor, with frequency as the parameter.

The Nyquist plot of an ideal linear-single-degree-of-freedom system with viscous damping is a generally circular plot as shown in Fig. 12. The plot originates at the point  $(1, 0)$  at zero frequency and circles to the origin as the frequency increases indefinitely. As noted previously, the natural frequency corresponds to the frequency near the peak quadrature response. The damping is related to the rate of change of frequency along the plot near the peak quadrature response, and with the damping known, the system mass is determined by the diameter of the circular plot.

For multiple-degree-of-freedom systems the Nyquist plot is the sum of the circular plots corresponding to each mode, and it generally consists of a number of loops as indicated in Fig. 13. With a fluid system each loop corresponds to a slosh mode and the entire plot is shifted to the right by the fraction of the total fluid mass (the residual mass) that does not take part in the vibration. If the individual modes are reasonably separated so that the loop for each mode is well defined, then the dynamic parameters for each mode can be estimated from the characteristics of its loop. The parameter

values for the i-th mode are defined below in terms of the symbols defined in Fig. 13.

$$\begin{aligned} \text{Natural frequency} &\approx f_0 \\ \text{Damping ratio } (\gamma = c/c_c) &= \frac{f - f_0}{f_0} \left( \frac{y}{x} \right) \\ \text{Mass fraction } (\mu) &= 2\gamma D \end{aligned} \tag{1}$$

The point defined by the frequency  $f$  is any point in the neighborhood of the local peak quadrature response, and the diameter  $D$  is for the circle that is the best fit in the neighborhood of the local peak quadrature response. To avoid the problem of metric mass units or U. S. customary weight units, the fluid mass associated with the i-th slosh mode is defined as a fraction of the total fluid mass. The mass fraction ( $\mu_i$ ) for the i-th mode is thus the ratio of the i-th slosh mass to the total fluid mass.

#### B. Parameter Optimization by Least Squares

When the individual modes are closely spaced in frequency, highly damped, or otherwise coupled, the loops of the Nyquist plot may not be well defined. Under these circumstances, parameter estimation based on the relationships in Eq. (1) becomes very approximate. This was found to be the case with the Nyquist plots obtained in the current slosh test and presented in Figs. 8 through 11.

To alleviate the problem, a nonlinear least squares curve fitting approach to parameter determination was developed. In this approach the theoretical Co-Quad response of an arbitrary N degree-of-freedom system was derived as a function of the system natural frequencies, damping ratios, and mass fractions (see the Appendix). At a specific driving frequency  $f$  the theoretical response is given by the following expressions:

$$\text{Co} \left( \frac{F}{m_T \ddot{x}} \right) = 1 + \sum_{i=1}^N \frac{\mu_i \Omega_i^2 (1 - \Omega_i^2)}{(1 - \Omega_i^2)^2 + 4\Omega_i^2 \gamma_i^2} \tag{2}$$

and

$$\text{Quad} \left( \frac{F}{m_T \ddot{x}} \right) = \sum_{i=1}^N \frac{-2\mu_i \Omega_i^3 \gamma_i}{(1 - \Omega_i^2)^2 + 4\Omega_i^2 \gamma_i^2} \quad (2)$$

where

$F/\ddot{x}$  = driving force/driving acceleration

$\mu_i$  = mass fraction of i-th mode  $\equiv m_i/m_T$

$\gamma_i$  = damping ratio of i-th mode  $\equiv (c/c_c)_i$

$\Omega_i$  = frequency ratio of i-th mode  $\equiv f/f_i$

$m_i$  = modal mass of i-th mode

$m_T$  = total fluid mass

$f$  = driving frequency

$f_i$  = natural frequency of i-th mode

Using the least squares approach, an error function was defined by summing the square of the difference between the theoretical and measured response over the set of  $p$  driving frequencies used in the test. More specifically, the error function is a function of the theoretical system state vector  $(\bar{a})$  and is given by:

$$E(\bar{a}) = \sum_{f=f_1}^{f_p} \left\{ \left[ \text{Co}_{\text{Theor}}(\bar{a}, f) - \text{Co}_{\text{Exp}}(f) \right]^2 + \left[ \text{Quad}_{\text{Theor}}(\bar{a}, f) - \text{Quad}_{\text{Exp}}(f) \right]^2 \right\} \quad (3)$$

where

$$\bar{a} \equiv \left[ \Omega_1, \Omega_2, \dots, \Omega_N, \gamma_1, \gamma_2, \dots, \gamma_N, \mu_1, \mu_2, \dots, \mu_N \right]$$

The state vector  $\bar{a}$ , which minimizes Eq. (3), defines the best fit dynamic parameter values.

To allow its application to future programs in addition to the current study, the above approach was implemented in the form of a general purpose computer program utilizing the variable metric method (Ref. 3) for the function minimization. The program NYQFIT was coded with a capacity of 1 to 10 modes (3 to 30 parameters) and up to 100 frequency response points. In addition, either structural or viscous damping was allowed. Computer costs were in the one-to-two-dollar range for cases with 5 degrees of freedom and around 30 frequency response points.

Experience with the program indicates that it is a very effective tool for Nyquist plot system analysis. One of its primary advantages is in indicating the response of the best ideal linear system approximation to the measured system. The difference between the closest theoretical system response and measured response is useful in indicating missing modes, system nonlinearities, and possible data errors. The dynamic parameters (natural frequencies, dampings, and mass fractions) associated with the closest theoretical system are, in themselves, useful in quantifying the measured system's characteristics.

### C. Parameter Estimates for Tested Tank

The relationships defined in Eqs. (1) were used to provide initial estimates of the system parameters from the measured Nyquist plots. The program NYQFIT was then used to optimize the parameters to obtain the best fit between the theoretical response and the measured response. Nearly 100 runs were made assuming both viscous and structural damping, and using various numbers of modes and various frequency ranges. Most work concentrated on the 0.1-, 0.3-, and 0.5-g excitation level data.

Figures 14 and 15 represent initial Nyquist plot fits for the 0.05 and 0.1-g data. The parameter values corresponding to the computer generated curves are indicated in the figures. The lack of agreement between the best fit theoretical response and the measured response indicates considerable system nonlinearity in the first two modes. In the measured response the first mode resonance appears to partially exclude the second mode resonance. Note that the loop associated with the measured first mode response is not

pulled as tight by the increasing second mode response as it is in the theoretical response.

In an attempt to improve the definition of the 0.1-g level first mode parameters, the first mode only was fitted with various single-degree-of-freedom models. This work indicated that the first mode natural frequency was about 3.2 Hz, and that the mass fraction was about 15%. When the data were incorporated into the overall 4 mode model, the 15% mass fraction was found to be inappropriate. As a final iteration the first mode natural frequency and mass fraction were held fixed while the remaining 10 parameters in the 4 mode model were optimized. This was done using various values for the first mode mass fraction. Typical results for the constrained optimization are presented in Fig. 16 for a first mode mass fraction of 25%. Together the data in Figs. 15 and 16 provide a quantitative estimate of the system parameter values, and the degree of system nonlinearity at the 0.1-g excitation level.

Attempts to fit the 0.3-g excitation level data with a single linear dynamic model were much less fruitful. It was quickly established that a single multiple-degree-of-freedom model could not be assumed across the entire frequency range. As described in Subsection V-B the diaphragm in the vibrating tank developed a completely different configuration during the primary 4.8-Hz resonance than it had outside the resonance. Accordingly, different models had to be used in the two frequency regions.

Figures 17 and 18 describe the results of fitting one- and two-degree-of-freedom models, respectively, to the primary 4.8-Hz resonance. As seen in Fig. 17 the single-degree-of-freedom model was unable to account for the response pattern in the region around 3 Hz. Based on the 0.1-g level response, which indicated a subdued resonance at about 3 Hz, it was concluded that the 0.3-g level response probably contained the same resonance hidden by the dominant 4.8-Hz mode. As indicated in Fig. 18 the two-degree-of-freedom model provided an excellent match for the measured data. However, the difference between various two-degree-of-freedom fits indicated that the subdued mode is not well defined. This is probably due to the fact that the diaphragm is changing shape in this region as the primary mode develops.

As described in Subsection V-B, the diaphragm jumps back to its original dimpled equilibrium shape as the frequency approaches 5 Hz. Figure 18 also contains a typical result of fitting 4-degree-of-freedom models to the response above 5 Hz. The first of the four degrees of freedom was used to account for the state of the tank at 5 Hz and was varied parametrically. Figure 18 represents the case where the first mode natural frequency and mass fraction were constrained to their best estimate values. The program was allowed to select the first mode damping as required to reach the starting point of the 7-Hz mode on the Nyquist plot.

Considering the 7-Hz mode, it appears to correspond to the 9-Hz mode at the 0.1-g level, reduced in frequency because of nonlinearities with excitation level. The high-order modes are similarly reduced in frequency and are generally quite similar to those indicated for the 0.1-g excitation level in Fig. 16.

At the 0.5-g excitation level the primary 4.8-Hz mode that developed at the 0.3-g level is essentially unchanged. Figure 19 represents the best fit to the 0.5-g data. Except for the presence of the small resonance around 9.6 Hz, which is considered to have been a fixture resonance, the response is quite similar to the response at the other levels. The primary difference is increased damping and slightly lower slosh frequencies.

Figures 20, 21, and 22 summarize the approximate variation of the modal parameters with increasing excitation level.

## VII. SUMMARY AND RECOMMENDATIONS

During the test program a 23-cm- (9-in. -) diam mercury propellant tank was tested with a 17.5% ullage volume. Emphasis was placed on establishing the general slosh behavior as a function of excitation level, and on deriving a computerized data reduction method. Natural frequencies, dampings, and modal masses were determined for the lateral slosh modes at sinusoidal excitation levels between 0.05 and 0.5 g peak. These data were reduced with the aid of a Nyquist plot least squares parameter fitting computer program that was coded as a general purpose tool suitable for use in future test programs.

The slosh response was found to be very dependent on the stiffness and deformed shape of the tank's positive expulsion diaphragm. As a result the response differed significantly from the theoretical response for the same fluid volume with a free surface. The response was also found to be very nonlinear with excitation level. At excitation levels above 0.2 g, the tank developed a new primary resonance that corresponded to a new deformed diaphragm shape different from the low-level equilibrium shape. Above this natural frequency the deformed shape jumped back to the low-level equilibrium shape. As a result the higher modes were less affected by the excitation level.

Because the current work concentrated on a single test configuration, the understanding of the slosh dynamics is not complete. Further testing will be required in the future to identify the significance and understand the effects of varying other slosh parameters. At this time the effect of tank size, ullage volume, ullage fluid, ullage pressure level, bladder stiffness, static acceleration field, and excitation direction is not adequately understood.

Some insight into the effect of larger ullages and more flexible diaphragms is given by Stofan and Pavli in Ref. 4. Their tests were conducted with a similar 24-cm-diam tank with diaphragm thicknesses of 0.25 and 0.5 mm, and ullage volumes of 50% and around 80%. As might be expected their data indicate much closer agreement with free surface slosh theory than the data presented here for a 1.6-mm thick diaphragm. However their data were obtained at constant excitation levels of 1.25 mm (0.05 in.) and 2.5 mm (0.10 in.). This corresponds to excitation levels of only about 0.01 and 0.02 g at 4 Hz. As indicated by this study, the results could be significantly different at flight levels that approach 1 g.

## APPENDIX

### DERIVATION OF THEORETICAL CO-QUAD RESPONSE

As indicated in Fig. A-1 the tank/fluid system is considered equivalent to a set of uncoupled single-degree-of-freedom oscillators plus two rigid masses. Each oscillator represents a slosh mode and is defined by its stiffness, mass, and damping. The rigid masses represent the mass of the tank and its moving support, and the residual mass of the fluid, which does not take part in the sloshing. Though the rotary inertia of the residual mass and the equivalent vertical positions of the slosh masses, noted in Fig. A-1, are of interest in a complete model of the fluid, only the lateral slosh behavior, which is independent of these parameters, is considered. For the total response of the model with both pitch and lateral excitation, including the height and inertia parameters, see Ref. 5. The following nomenclature is adopted:

$c_i$  = viscous damping factor for  $i$ -th mode

$F(t)$  = total lateral excitation force

$F_T$  = scaler amplitude of sinusoidal excitation force

$F$  = scaler amplitude of sinusoidal fluid reaction force

$g_i$  = structural damping factor for  $i$ -th mode

$i$  = index denoting the  $i$ -th slosh mode

$j$  =  $\sqrt{-1}$

$k_i$  = stiffness of  $i$ -th mode

$m_i$  = modal mass of  $i$ -th mode

$m_T$  = total fluid mass

$m_0$  = residual fluid mass =  $m_T - \sum m_i$

$M$  = mass of tank and related fixturing

$n$  = number of significant slosh modes

$t$  = time

$x_i$  = lateral displacement of  $m_i$  relative to the tank

$x_0$  = absolute displacement of tank relative to ground

$X_i$  = scaler amplitude of sinusoidal  $x_i$

$X$  = scaler amplitude of sinusoidal  $x_0$

$\ddot{X}$  = scaler amplitude of sinusoidal tank acceleration  $\ddot{x}_0$

$\gamma_i$  = damping ratio for  $i$ -th mode =  $(c/c_c)_i$

$\mu_i$  = mass fraction for  $i$ -th mode =  $m_i/m_T$

$\omega$  = frequency of sinusoidal excitation

$\omega_i$  = natural frequency of  $i$ -th mode

$\Omega_i$  = frequency ratio of  $i$ -th mode =  $\omega/\omega_i$

$\sum_i$  = summation over  $i$  for  $i = 1, n$

Writing Newton's second law for the lateral motion of the total tank/fluid system gives

$$F(t) = (M + m_0)\ddot{x}_0 + \sum m_i(\ddot{x}_0 + \ddot{x}_i) \quad (A-1)$$

and for the  $i$ -th slosh mass gives

$$-k_i x_i - c_i \dot{x}_i = m_i(\ddot{x}_0 + \ddot{x}_i)$$

or

$$m_i \ddot{x}_i + c_i \dot{x}_i + k_i x_i = -m_i \ddot{x}_0 \quad (A-2)$$

For steady state sinusoidal tank motion:

$$\begin{aligned}
 F(t) &= F_T \exp(j\omega t) \\
 \ddot{x}_0 &= \ddot{X} \exp(j\omega t) \\
 x_i &= X_i \exp(j\omega t) \\
 \dot{x}_i &= j\omega X_i \exp(j\omega t) \\
 \ddot{x}_i &= -\omega^2 X_i \exp(j\omega t) = \ddot{X}_i \exp(j\omega t)
 \end{aligned}
 \tag{A-3}$$

Substituting into Eq. (A-2) gives

$$\ddot{X}_i = \frac{\omega^2 m_i \ddot{X}}{-\omega^2 m_i + j\omega c_i + k_i}
 \tag{A-4}$$

Substituting Eqs. (A-3) and (A-4) into Eq. (A-1) and factoring out the tank acceleration gives:

$$F_T \exp(j\omega t) = \left[ M + m_0 + \sum_i m_i + \sum_i \left( \frac{m_i^2 \omega^2}{-\omega^2 m_i + j\omega c_i + k_i} \right) \right] \ddot{X} \exp(j\omega t)
 \tag{A-5}$$

or

$$\frac{F_T}{\ddot{X}} - M = m_T + \sum_i \left( \frac{m_i \omega^2}{\frac{k_i}{m_i} - \omega^2 + \frac{j\omega c_i}{m_i}} \right)
 \tag{A-6}$$

Now define

$$F = F_T - M\ddot{X}$$

$$\omega_i^2 = \frac{k_i}{m_i}$$

$$\gamma_i = \left( \frac{c}{c_c} \right)_i = \frac{c_i}{2m_i\omega_i} \quad (\text{A-7})$$

$$\Omega_i = \frac{\omega}{\omega_i}$$

$$\mu_i = \frac{m_i}{m_T}$$

Substituting the definitions of Eqs. (A-7) into Eq. (A-6) gives

$$\frac{F}{\ddot{X}m_T} = 1 + \sum_i \frac{\mu_i\Omega_i^2}{1 - \Omega_i^2 + 2j\gamma_i\Omega_i} \quad (\text{A-8})$$

Separating Eq. (A-8) into its real (Co) and imaginary (Quad) components gives:

$$\text{Co} \left( \frac{F}{\ddot{X}m_T} \right) = 1 + \sum_i \frac{\mu_i\Omega_i^2(1 - \Omega_i^2)}{(1 - \Omega_i^2)^2 + 4\gamma_i^2\Omega_i^2} \quad (\text{A-9})$$

$$\text{Quad} \left( \frac{F}{\ddot{X}m_T} \right) = \sum_i \frac{-2\mu_i\gamma_i\Omega_i^3}{(1 - \Omega_i^2)^2 + 4\gamma_i^2\Omega_i^2} \quad (\text{A-10})$$

which is the desired solution for viscous damping. For structural damping the result is identical to the above except that the viscous damping factor  $\gamma_i$  is replaced by

$$\gamma_i = \frac{g_i}{2\Omega_i} \quad (\text{A-11})$$

where  $g_i$  is the structural damping factor for the  $i$ -th slosh mode.

## REFERENCES

1. Masek, T. C., Solar Electric Propulsion Thrust Subsystem Development, Technical Report 32-1579. Jet Propulsion Laboratory, Pasadena, Calif., March 31, 1973.
2. Abramson, H. N., The Dynamic Behavior of Liquids in Moving Containers. NASA SP-106, Scientific and Technical Information Division, National Aeronautics and Space Administration, Washington, D. C., 1966.
3. Fletcher, R., and Powell, M. J., "Rapidly Convergent Descent Methods for Minimization," Comput. J., Vol. 7, pp. 149-154, July 1964.
4. Stofan, A. J., and Pavli, A. J., Experimental Damping of Liquid Oscillations in a Spherical Tank by Positive-Expulsion Bags and Diaphragms. NASA Technical Note D-1311, Lewis Research Center, Cleveland, Ohio, July 1962.
5. Abramson, H. N., Chu, W., and Ransleben, G. E., "Representation of Fuel Sloshing in Cylindrical Tanks by an Equivalent Mechanical Model," ARS J., Vol. 31, pp. 1697-1705, Dec. 1961.

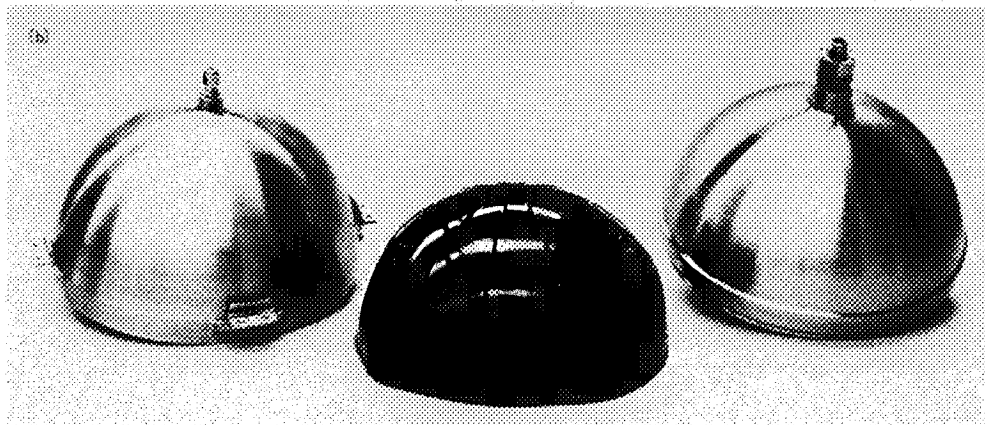
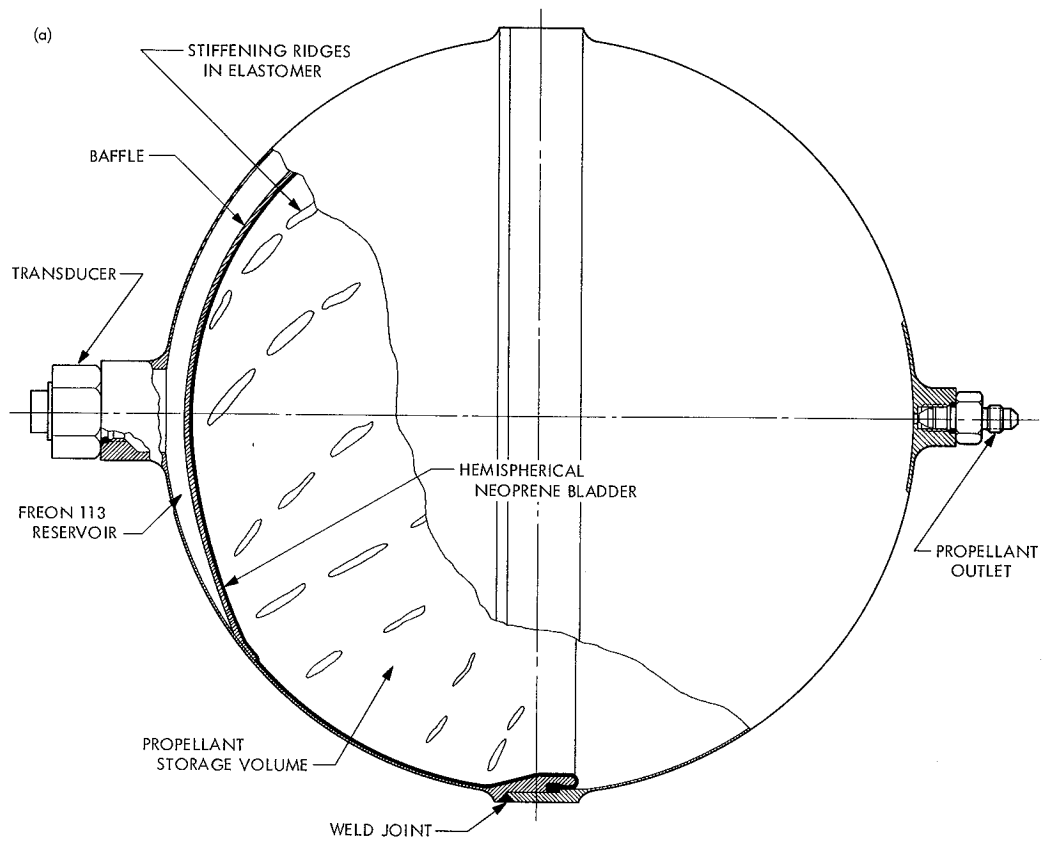


Fig. 1. SEPST Program propellant tank design (propellant-loaded position):  
 (a) line drawing; (b) disassembled mercury propellant tank

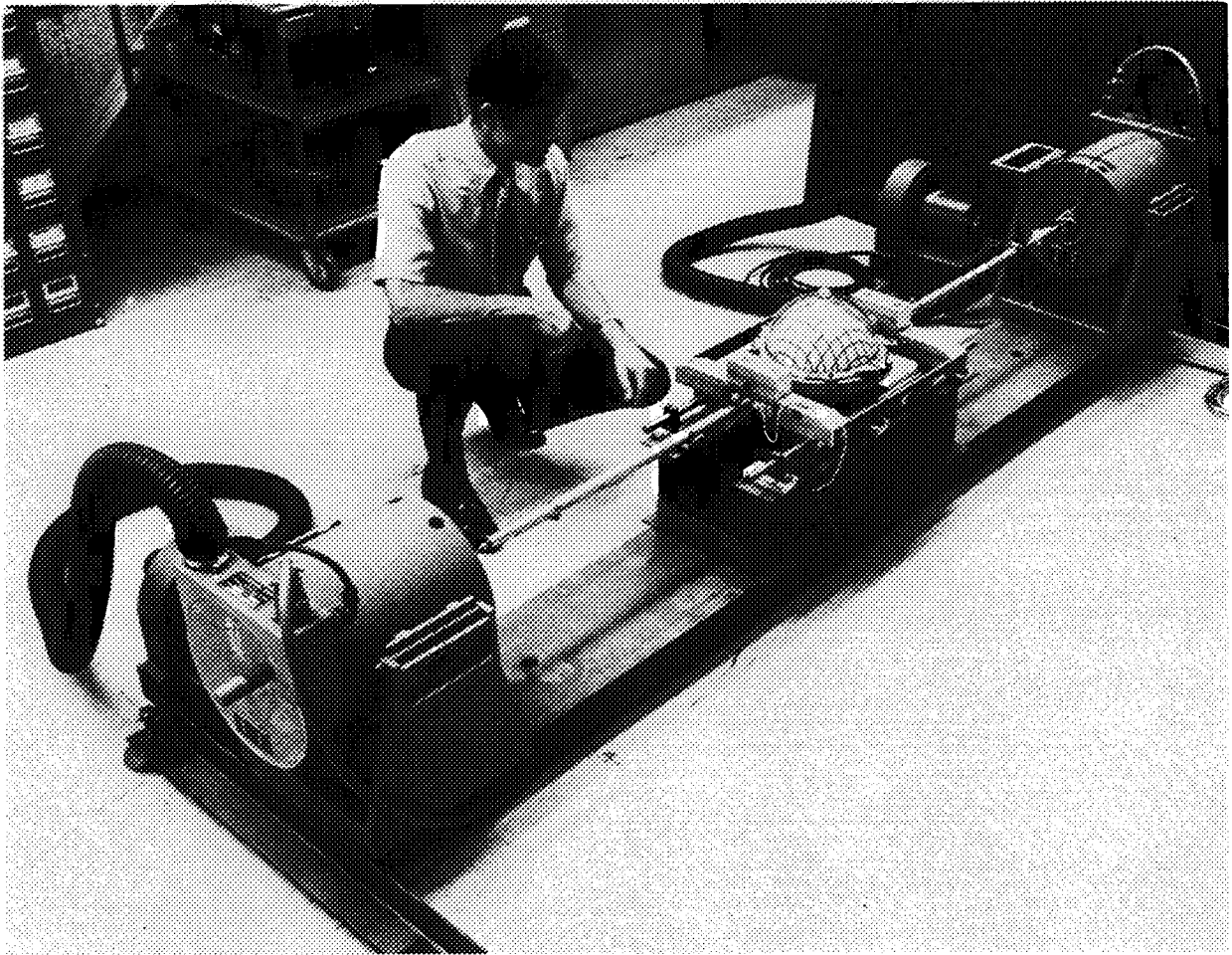


Fig. 2. Test tank mounted in sloshing apparatus

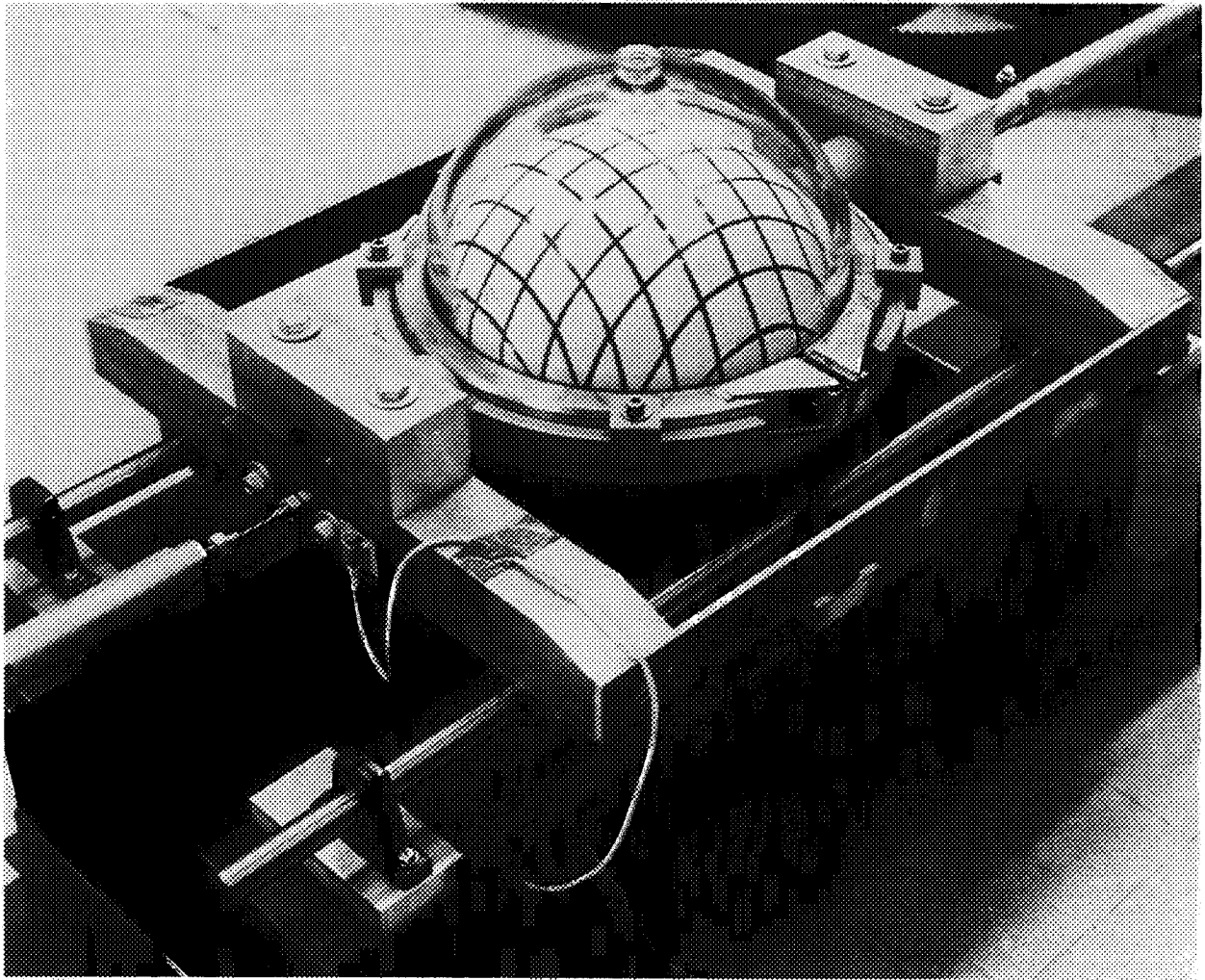


Fig. 4. Test tank with water (17.5% ullage)

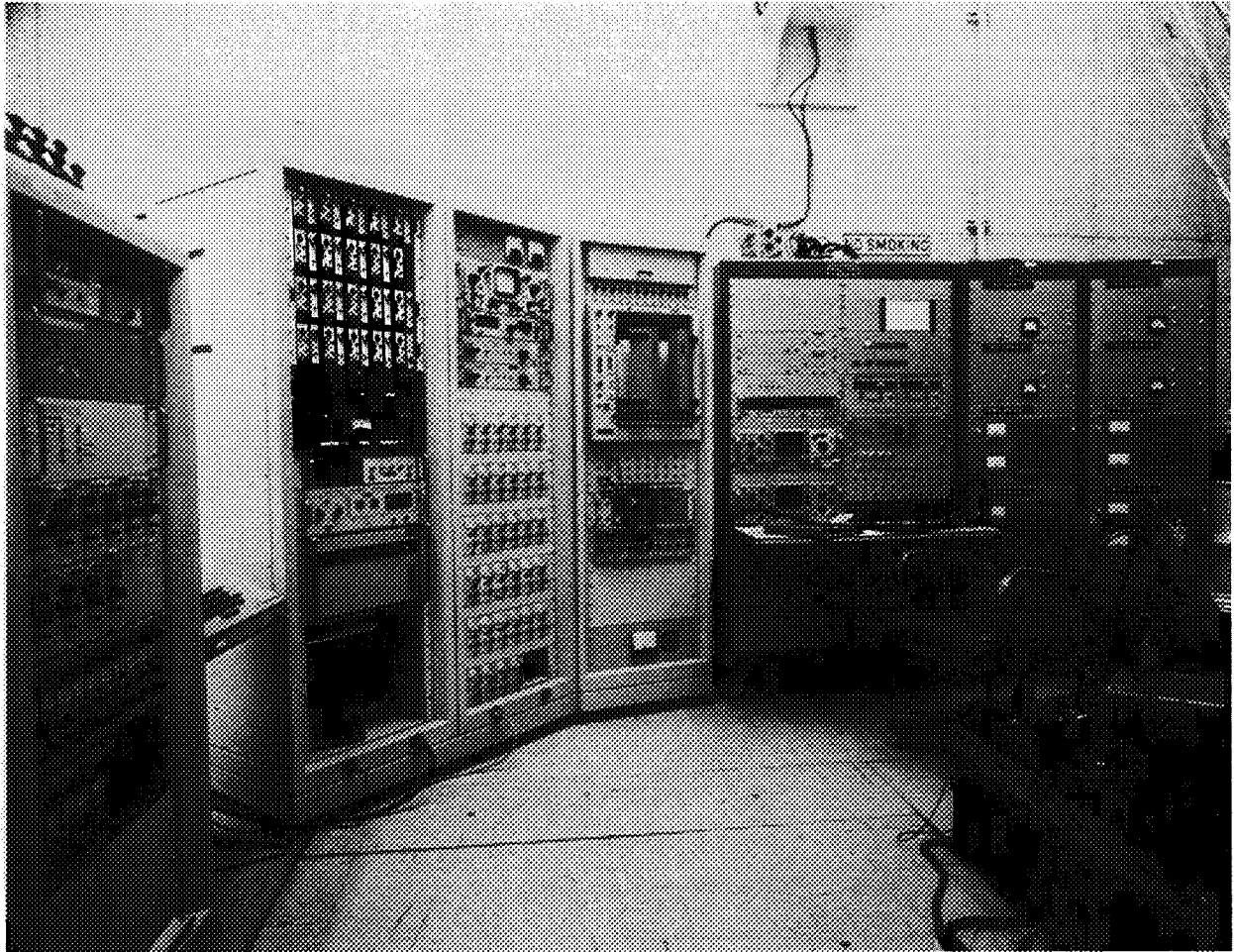


Fig. 3. Shaker control and data processing console

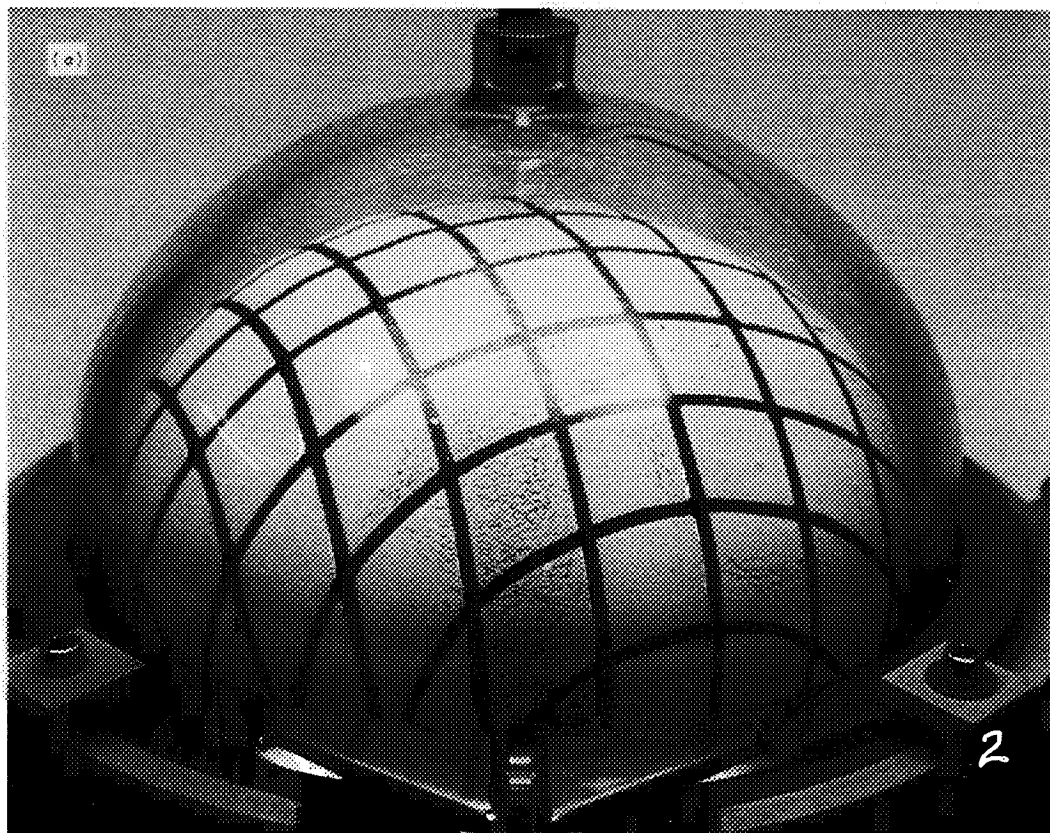


Fig. 5. Static diaphragm shapes with mercury for various ullages:  
(a) 90% ullage; (b) 80% ullage; (c) 70% ullage; (d) 60% ullage

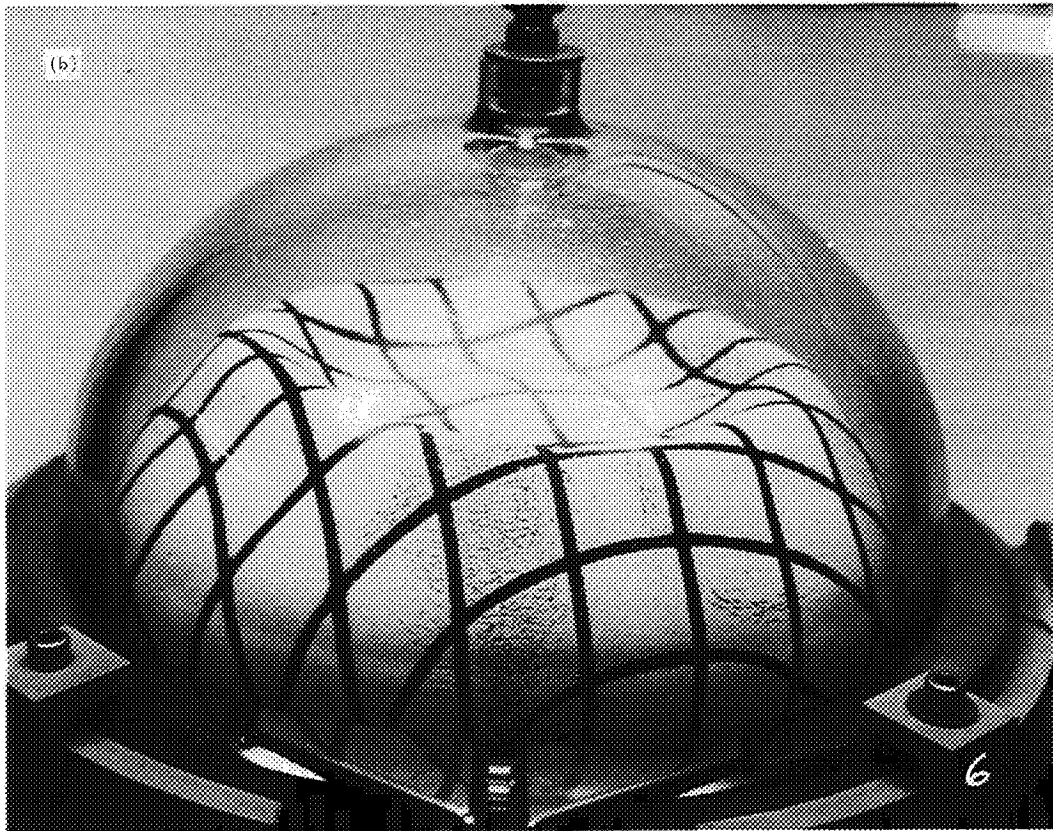


Fig. 5 (contd)

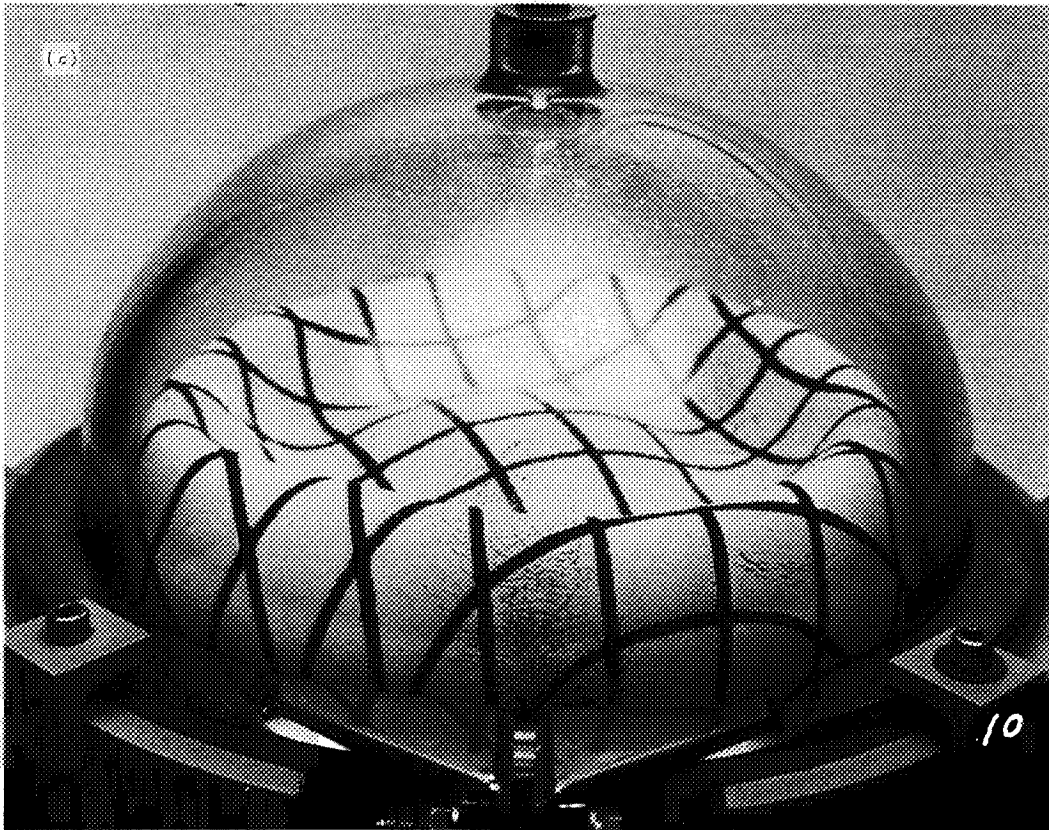


Fig. 5 (contd)

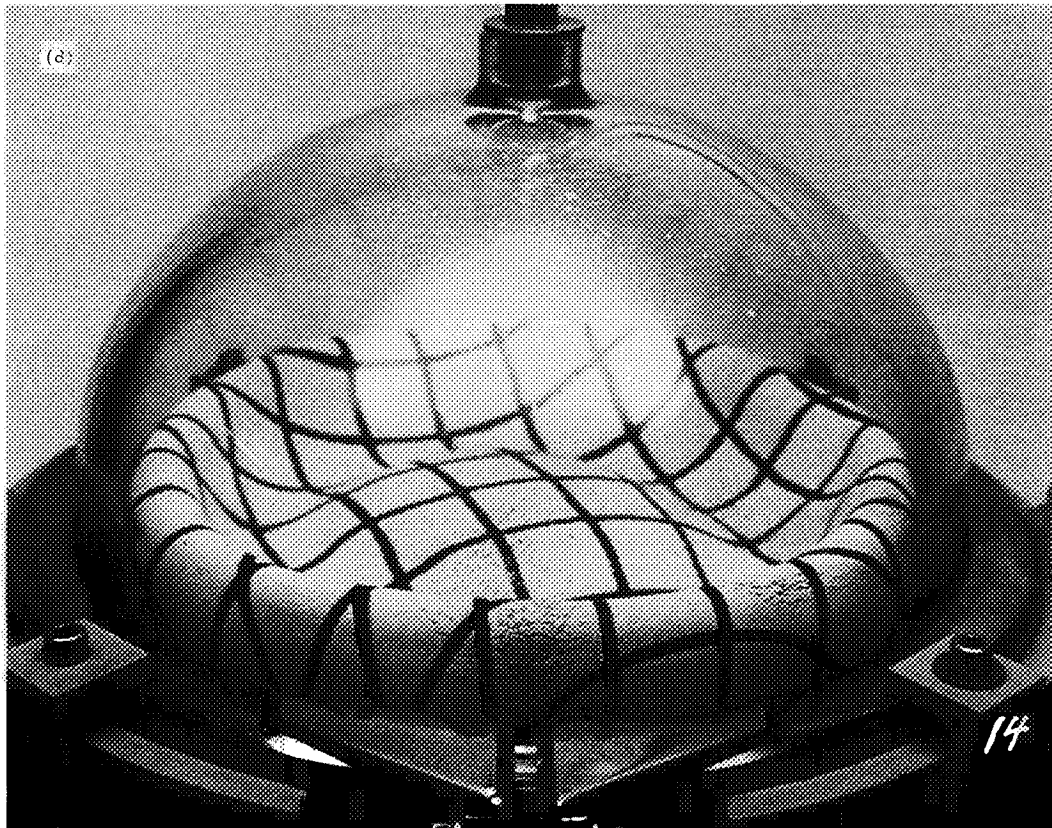


Fig. 5 (contd)

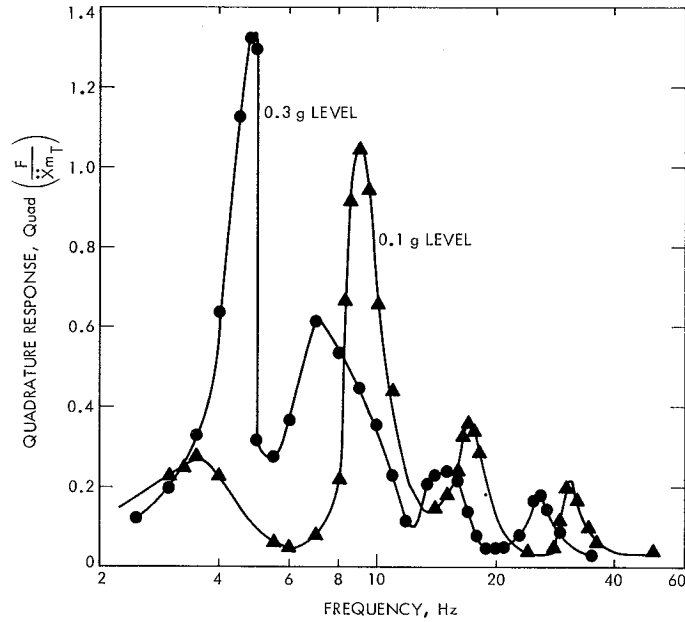


Fig. 6. Quadrature response of test tank with mercury

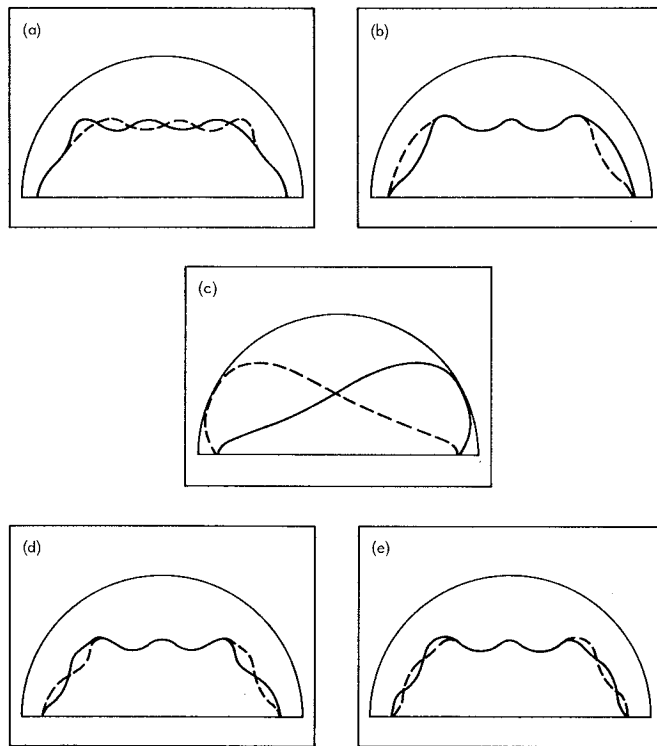


Fig. 7. Approximate mode shapes for mercury resonances: (a) first mode, 3 Hz; (b) second mode, 8 Hz; (c) high-level primary mode, 4.8 Hz; (d) third mode, 15 Hz; (e) fourth mode, 30 Hz

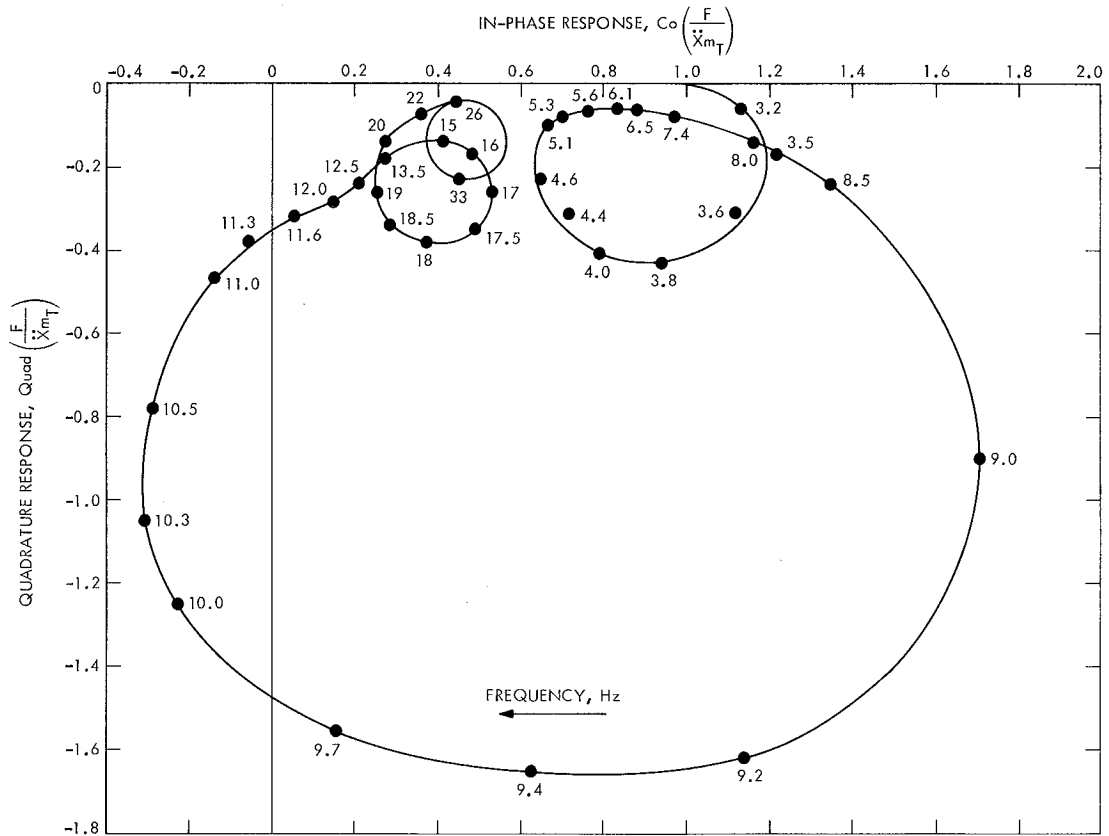


Fig. 8. Nyquist plot for 0.05 g excitation level

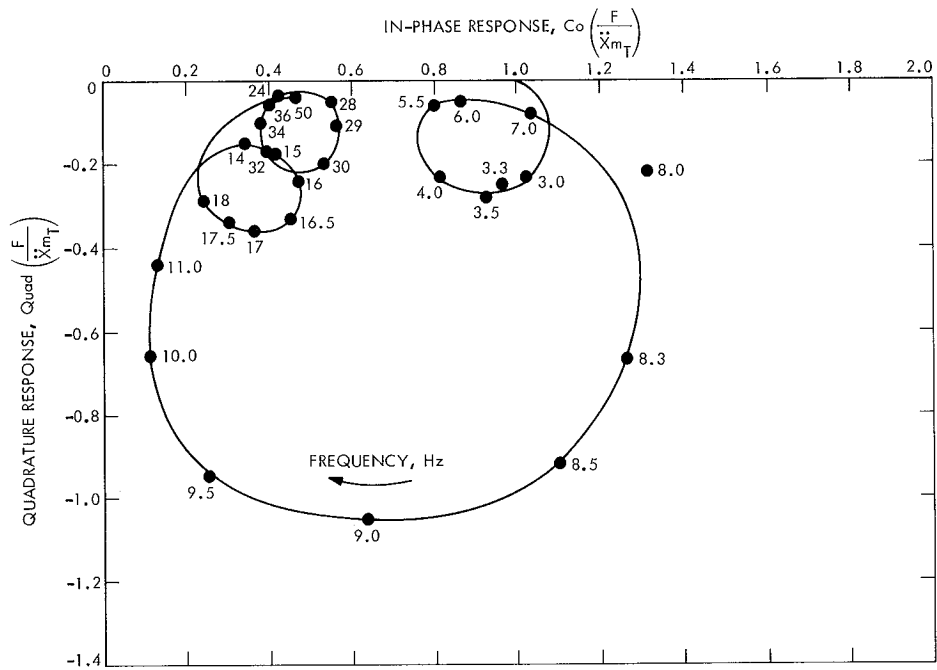


Fig. 9. Nyquist plot for 0.1 g excitation level

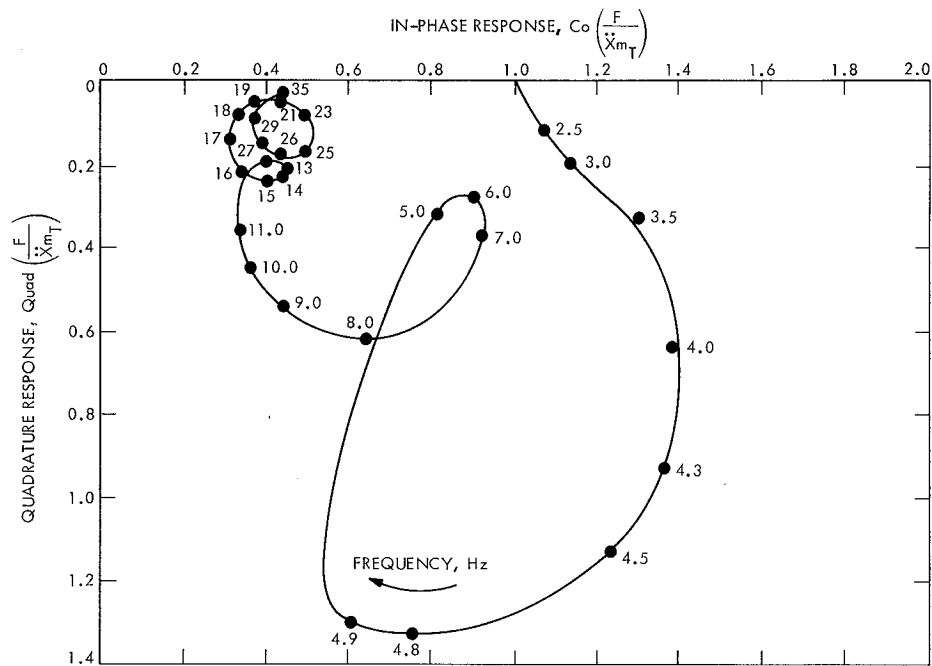


Fig. 10. Nyquist plot for 0.3 g excitation level

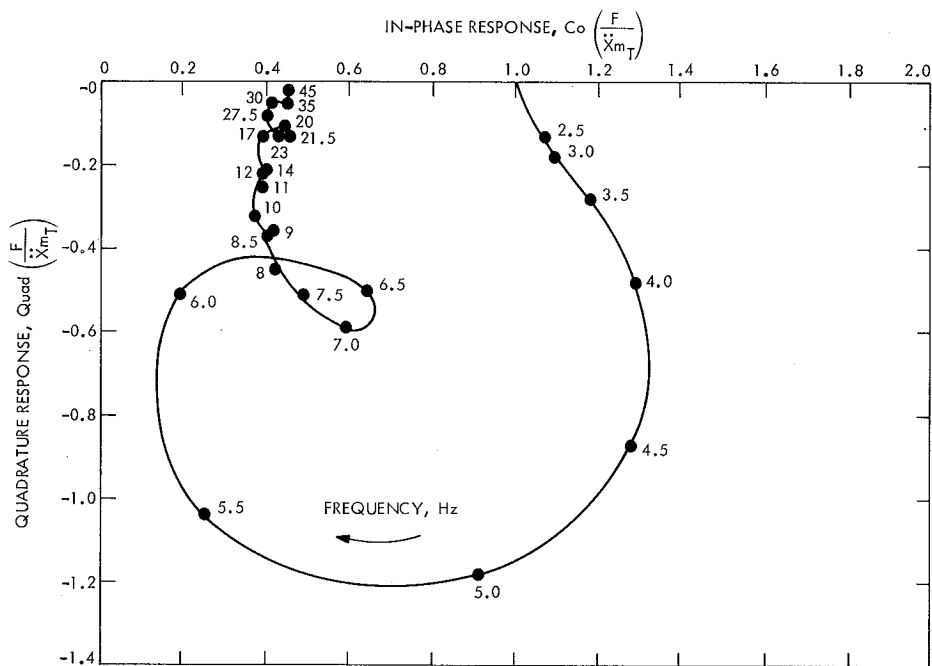


Fig. 11. Nyquist plot for 0.5 g excitation level

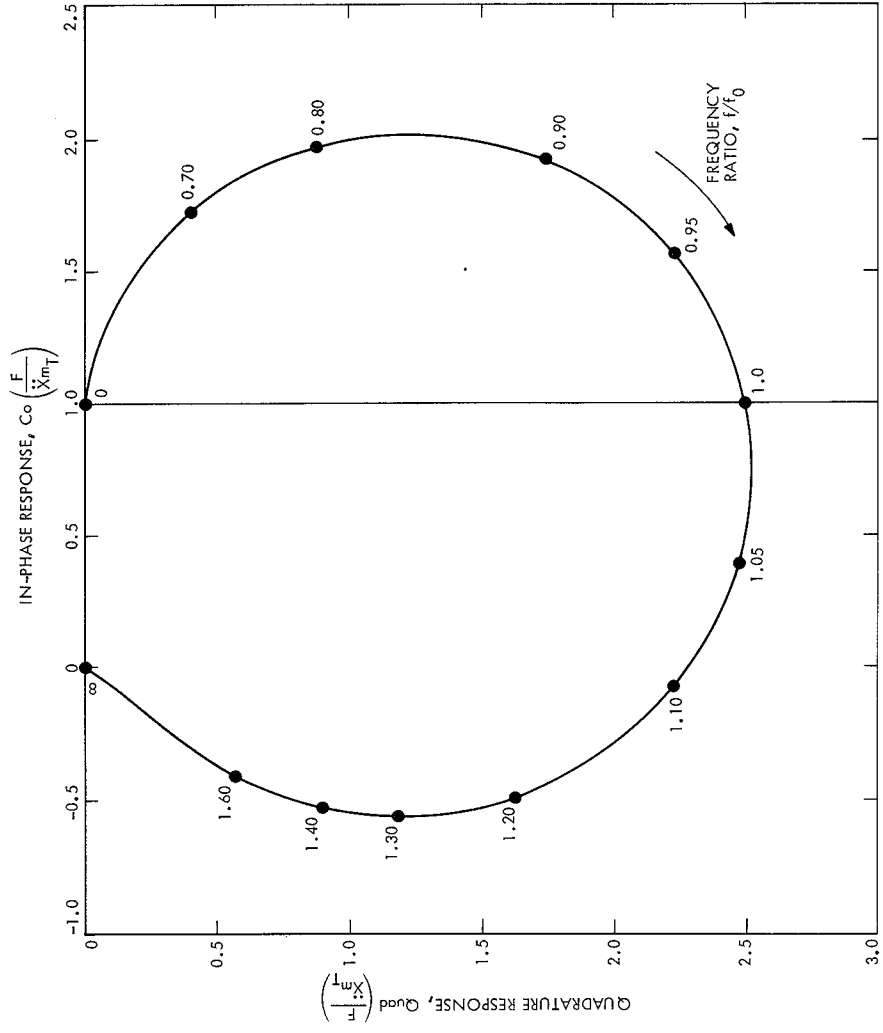


Fig. 12. Typical Nyquist plot for single-degree-of-freedom system ( $f_0 = 1$ ,  $\gamma = 0.2$ ,  $\mu = 1.0$ )

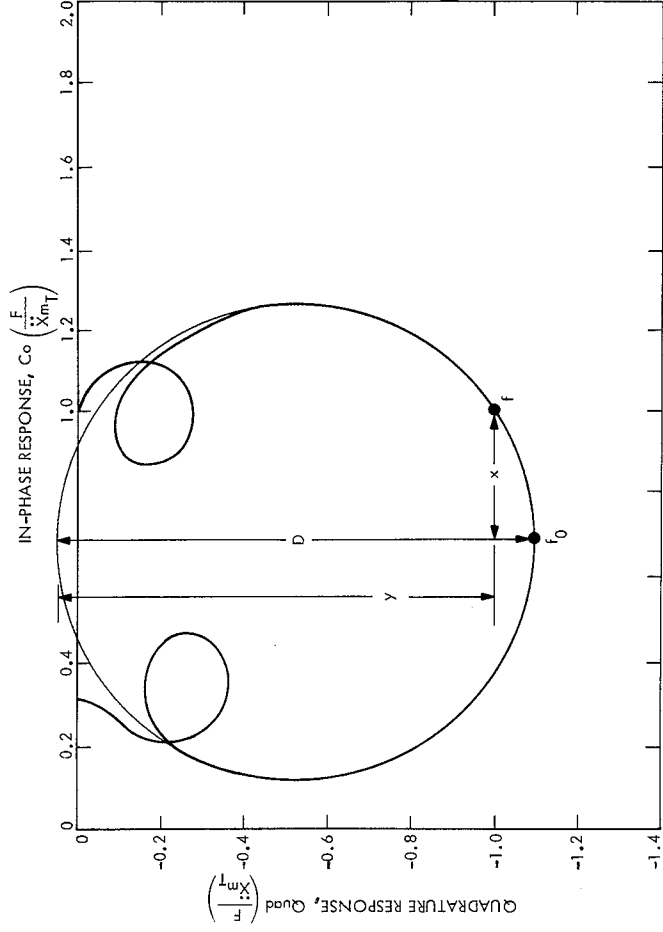


Fig. 13. Typical Nyquist plot for multiple-degree-of-freedom system

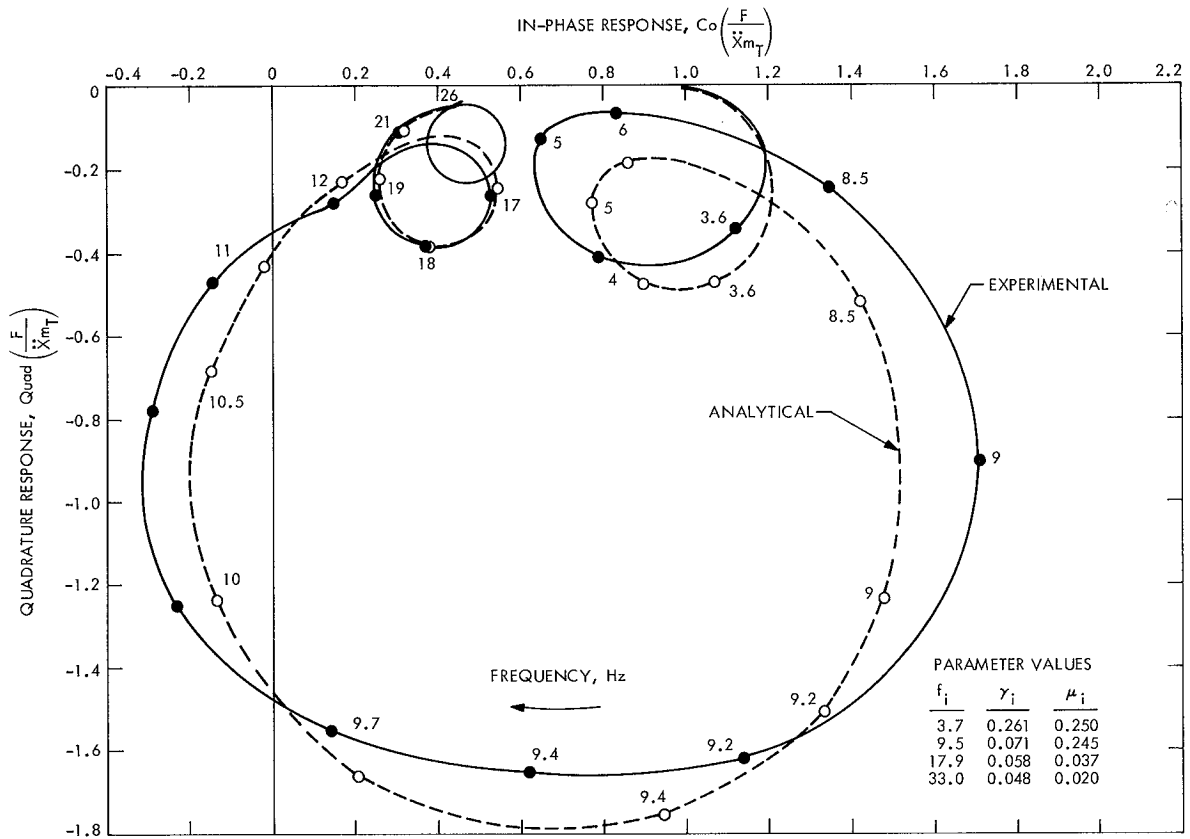


Fig. 14. Initial linear system fit for 0.05 g data

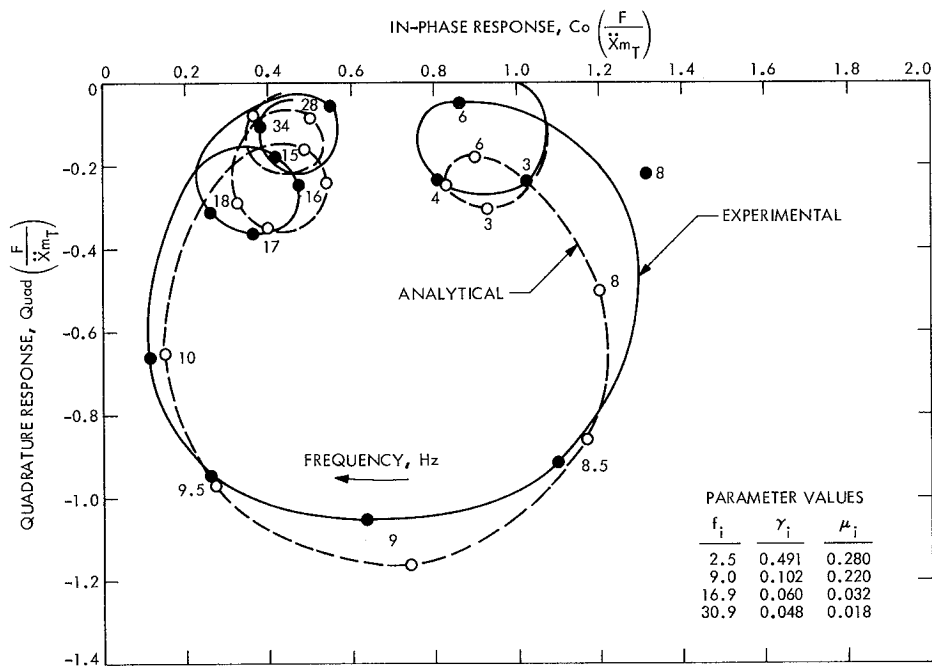


Fig. 15. Initial linear system fit for 0.1 g data

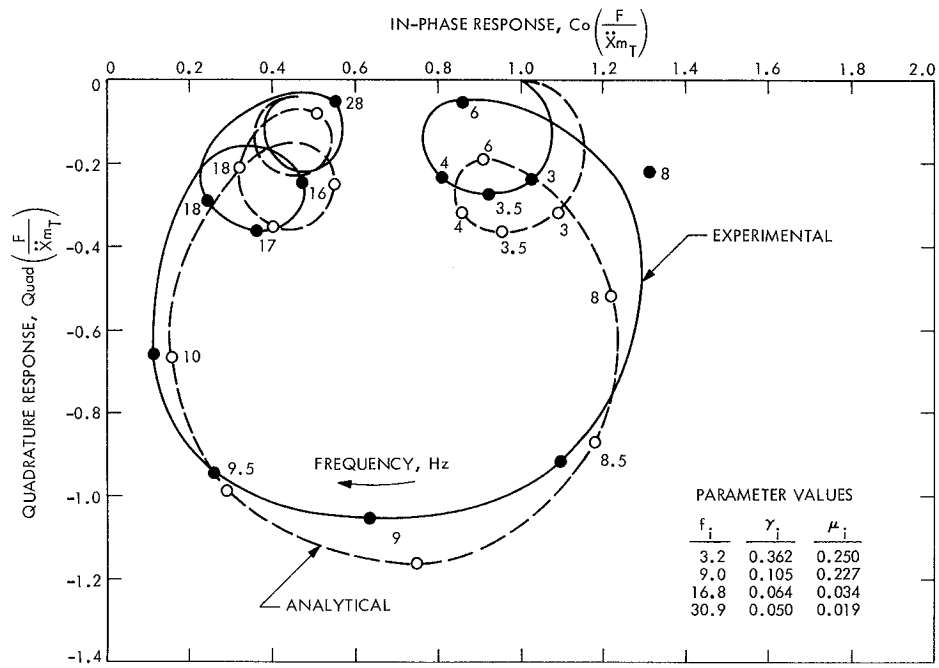


Fig. 16. Optimized linear system fit for 0.1 g data

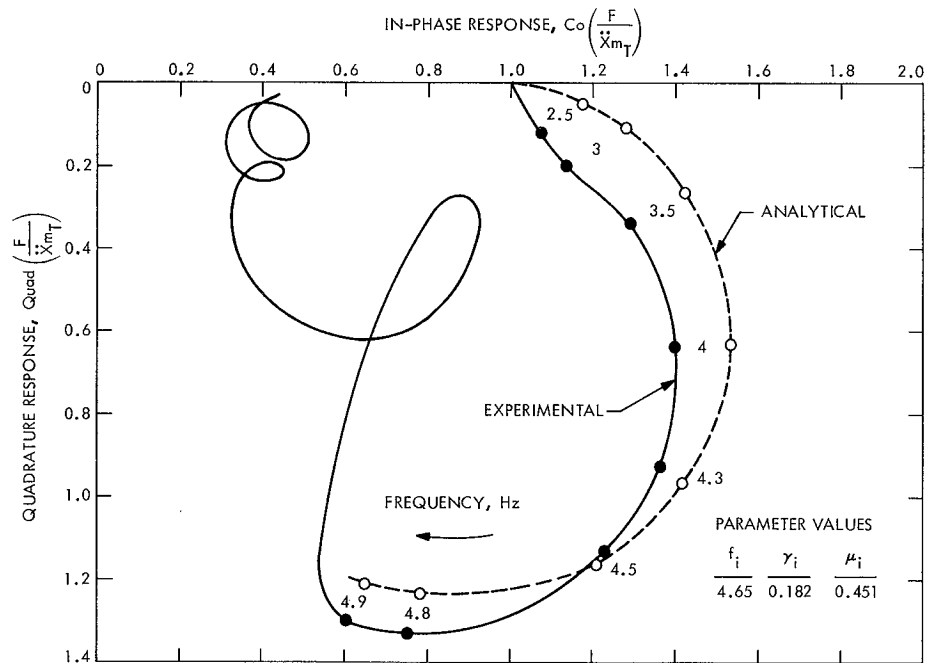


Fig. 17. Initial single-degree-of-freedom fit for 0.3 g primary resonance

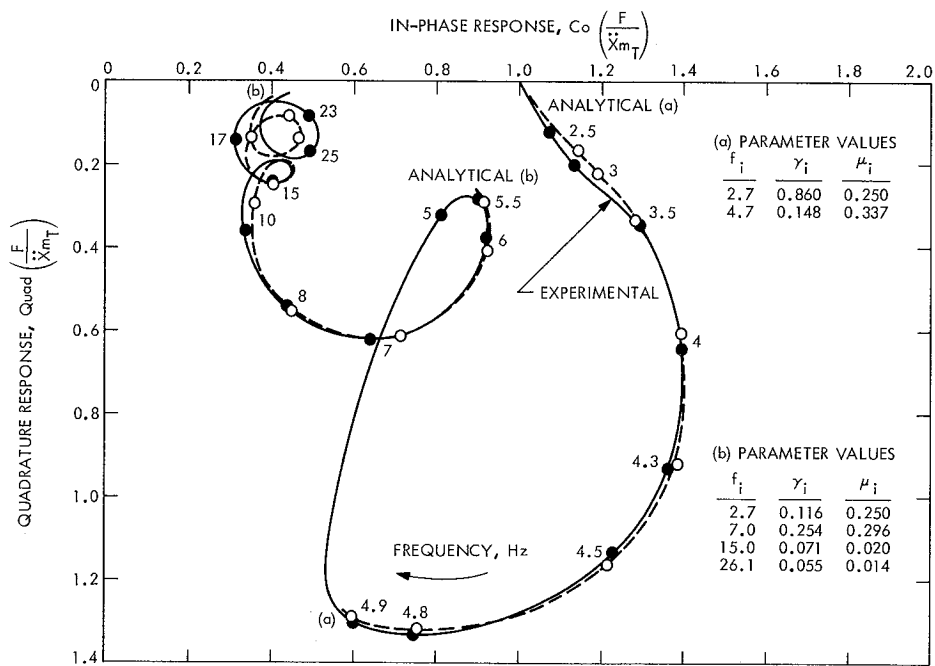


Fig. 18. Optimized linear system fit for 0.3 g data

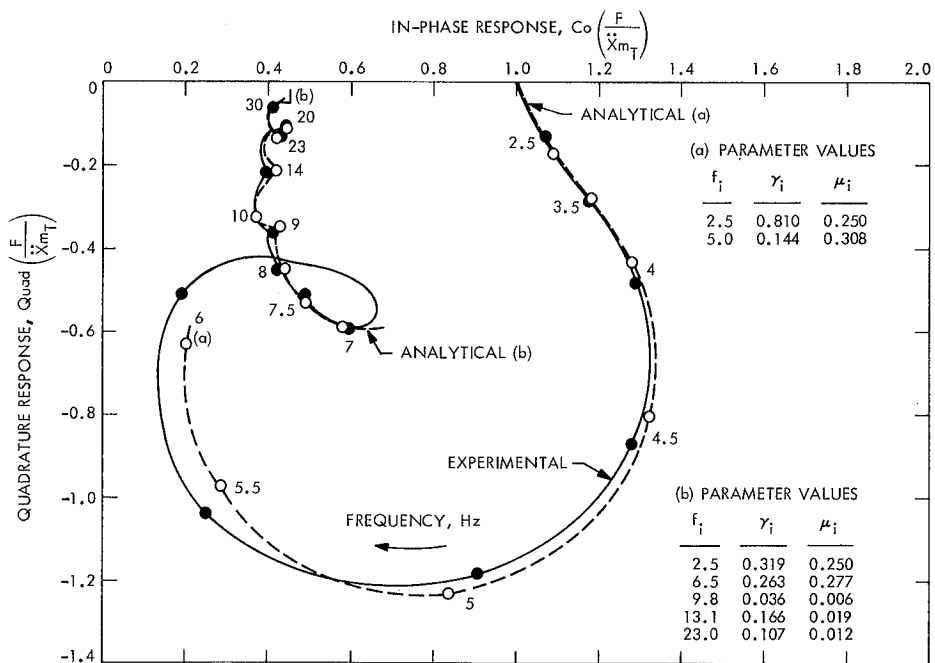


Fig. 19. Optimized linear system fit for 0.5 g data

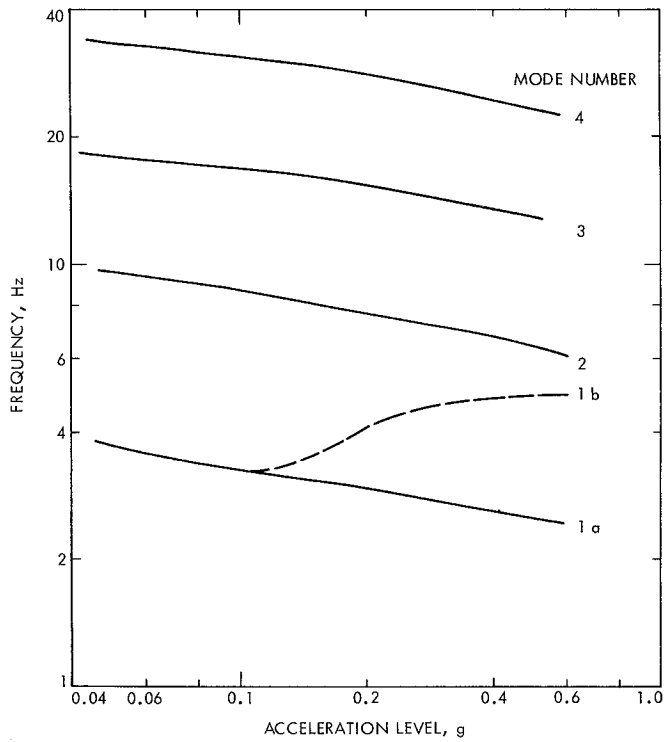


Fig. 20. Natural frequency versus excitation level

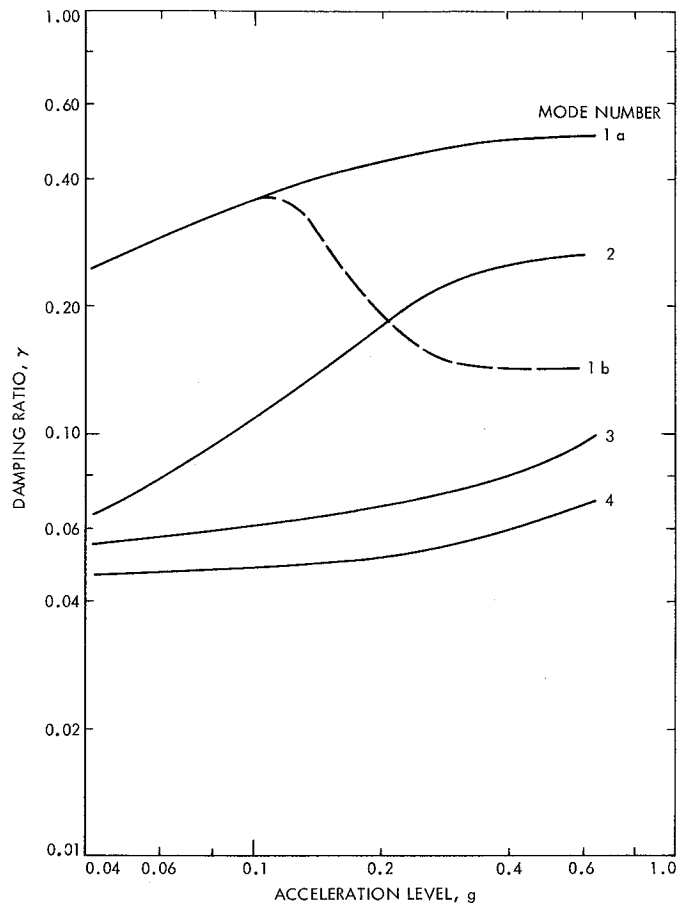


Fig. 21. Damping ratio versus excitation level

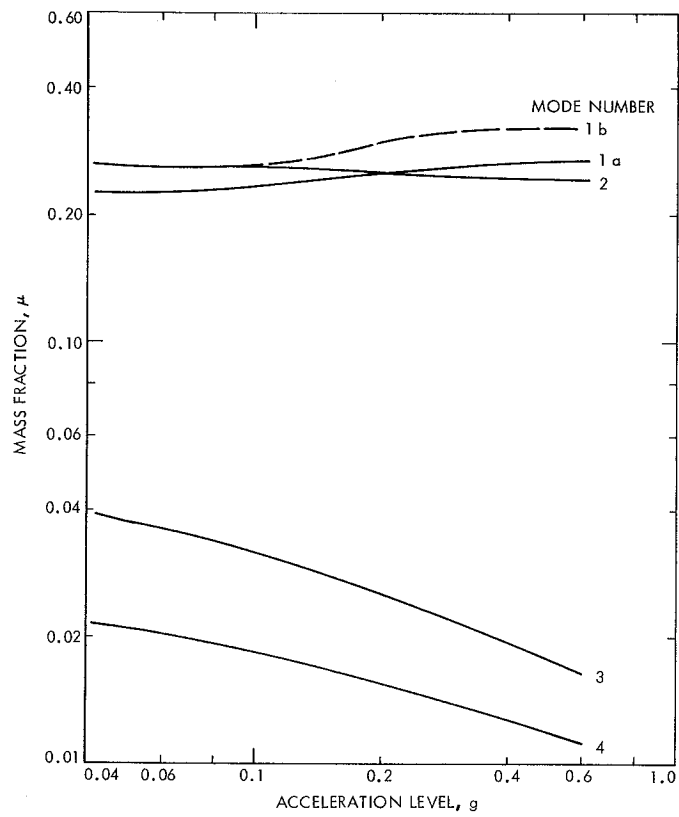


Fig. 22. Mass fraction versus excitation level

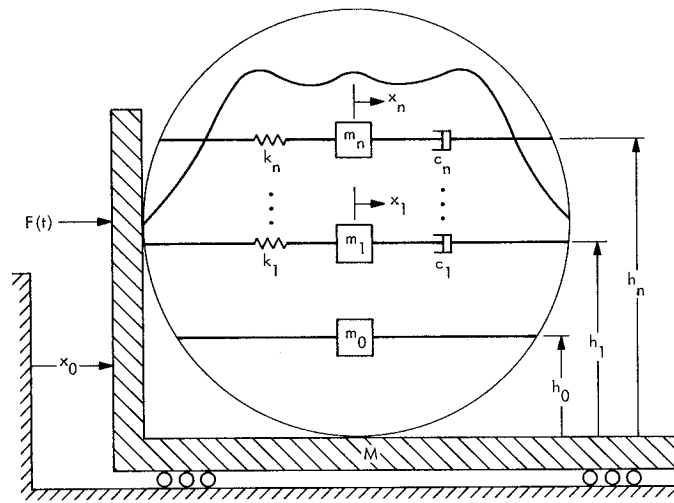


Fig. A-1. Dynamic model of tank/fluid system

